2017 International Conference on Indoor Positioning and Indoor Navigation (IPIN), 18-21 September 2017, Sapporo, Japan

Scalable and Precise Multi-UAV Indoor Navigation using TDOA-based UWB Localization

Janis Tiemann and Christian Wietfeld
TU Dortmund University, Communication Networks Institute (CNI)
Otto-Hahn-Str. 6, 44227 Dortmund, Germany
{janis.tiemann and christian.wietfeld}@tu-dortmund.de

***Abstract*—Ultra-wideband wireless positioning technologies based on IEEE 802.15.4a have gained attention for various use cases requiring highly precise localization. Multi-rotor unmanned aerial vehicle (UAV) systems provide several sensors for stabilization and navigation. However, absolute indoor positioning poses a problem for autonomous robotic systems. The specific challenge addressed in this paper is enabling novel applications with autonomous UAV systems through tight integration with scalable and precise receiver-side time-difference of arrival (TDOA) based ultra-wideband (UWB) indoor localization. For the in-depth validation of the proposed approach, several experiments are performed. One proves the repeatability of the proposed method by following a predefined trajectory ten times achieving close to optical motion-capture based control performance, with a 3rd quartile of the alignment error lower than 10 cm. Another experiment addresses the simultaneous flight of three UAVs in close proximity and delivers an analysis of the real-time capabilities which in turn proves the multi-user scalability. The last experiment demonstrates a user-interactive application of the proposed approach in a logistics environment. A video along with the raw samples, reference data and processed positions of the aforementioned experiments is provided alongside this work.**

Keywords*—Ultra-wideband (UWB), Time-Difference of Arrival (TDOA), Wireless Clock Synchronization, Unmanned Aerial Vehicle (UAV).

I. Introduction and Related Work

Quadrotors have been involved in a lot of research activities in the recent years. Testbeds for flying robots using professional and highly expensive optical motion tracking systems such as [1], [2], [3] and [4] gained significant attention.

Recent developments in affordable ultra-wideband (UWB) transceivers however, enabled high precision time of arrival (TOA) measurements in wireless communication. Those capabilities challenged a significant amount of research. Due to the limitations of optical motion capture systems in cost, space of operation and light conditions, the use of recent wireless positioning technology is close at hand for quadrotor position control. The research of Kempke et al. [5] [6] uses quadrotors as a platform to evaluate the accuracy of their UWB positioning system. However, quadrotor control through the system inputs is not investigated. In [7] the UWB positioning system is used as a reference for an optical flow sensor system, but not as a basis for actual position control. Hausman et al. [8] presented multi-sensor fusion of optical, global navigation satellite (GNSS), UWB and inertial measurement unit (IMU) data to improve the positioning quality of quadrotor unmanned aerial vehicles (UAV) in starting and landing scenarios. A commercial UWB system from *Time Domain* was used to improve positioning data locally. UAV position control based on the fused positioning data however was not stated to be part of that work.

978-1-5090-6299-7/17/$31.00

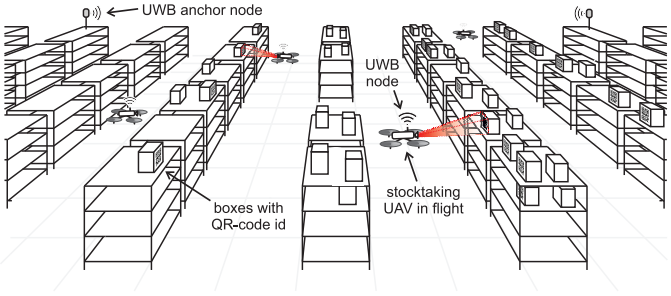

Fig. 1. Illustration of an indoor navigation application. UAVs are used for fast and flexible automated stocktaking in a warehouse by scanning the good's QR-codes. The localization system determines the positions of the drones through the time-differences of arrival of the frames received at the anchor nodes.

Guo et al. also present the integration of a commercial sytem from *Time Domain* to enable autonomous UAV flight using UWB, see [9]. However, the proposed integration is based on two-way ranging (TWR), a method that requires the exchange of two to four messages per mobile node for each anchor node. Therefore, TWR without coordination has limited scalability in terms of channel access. Mueller et al. [10] proposed a system based on UWB using TWR with the special extension of multiple acknowledgments (TWR-MA). Multiple acknowledgments are used to compensate for the individual clock drift of the ranging nodes while avoiding the reporting necessary after symmetric double-sided two-way ranging (SDS-TWR) to obtain the ranging information at the mobile unit. Ledergerber et al. [11] used a more multi-user scalable time-difference of arrival (TDOA) based positioning scheme, where the anchors transmit in defined intervals. In both schemes the quadrotor receives all necessary information to compute its position locally on an *Ascending Technologies Hummingbird* quadrotor with a modified *Pixhawk PX4* flight management unit. However, although providing infinite multi-user scalability the authors state that through imperfect anchor clock synchronization the positioning errors are larger than expected.

In contrast to the prior mentioned examples, this work provides an approach combining precise localization with multi-user scalablility through the use of a receiver-side TDOA topology, initially presented in [12]. The initial motivation for the application was the integration of black-box UAV systems

into indoor search and rescue environments. This was achieved by the emulation of typical GNSS receivers exploiting the serial interface used by the receiver to communicate with the flight controller. However, when trying to use multiple UAVs, multi-user scalability of SDS-TWR based ranging that was used, in previous work [13], turned out to be very inefficient in terms of channel utilization per obtained position. Therefore, an open-source TDOA-based UWB localization system [14] using wireless clock synchronization detailed in [12] was developed to overcome the multi-user limitations of previous work.

In this paper we will present a multi-user scalable but also precise integration of low-cost consumer-grade UAVs into the indoor environment to a level where the usage in productive applications such as a stocktaking process, see Fig. 1, is enabled. This paper proves the capabilities of the approach through a simultaneous flight of three UAVs in a challenging space-constraint environment overcoming the limitations of TWR-based systems.

II. Proposed System Implementation

The experimental system is based on the *Parrot Bebop*, which is a highly integrated low-cost drone. In the context of this work, this drone was slightly modified to host the power supply for an on-board UWB node, see Fig. 2. In the standard configuration, the drone uses WLAN based on IEEE 802.11ac in access point mode to communicate to an end-user device. In order to enable multi-drone scenarios, the WLAN configuration was modified from access point mode to client mode over an on-board debugging connector hidden to consumer users. The drone runs a Linux-based operating system and features several sensors:

- Accelerometer, Gyroscope (*InvenSense MPU-6050*)
- Magnetometer (*AsahiKASEI AK8963*)
- Optical-flow sensor (Lateral velocity estimation)
- Ultrasound sensor (Height above ground estimation)
- Pressure sensor (*Measurement Specialties MS5607*)
- GNSS receiver (*Furuno GN-87*)

The software development kit (SDK) provided by Parrot does not provide raw sensor data. Nevertheless, an abstract representation of the sensor readings in form of already fused odometry information is available.

The system topology of the overall experimental setup is depicted in Fig. 3. The Robot Operating System (ROS) [15] is used as the central component, interfacing all individual parts comprising the setup in a flexible and modular way. Control and feedback of the drone was handled through the *bebop_autonomy* ROS driver developed by Monajjemi et al., see [16]. A motion capture system with a set of eight *OptiTrack Flex13* cameras was used as a ground-truth for determining the positioning error of the UWB system. It was also used in the development stage to tune the position control of the drones. The ROS interface was handled by the *mocap_optitrack* package, translating the specific motion capture streaming data to ROS-compatible messages. The ROS package *visp_auto_tracker* [17] was used to process image data from the drone's camera to enable QR-code detection for interactive demonstration.

Fig. 2. Modified Parrot Bebop 1st generation used in this work.

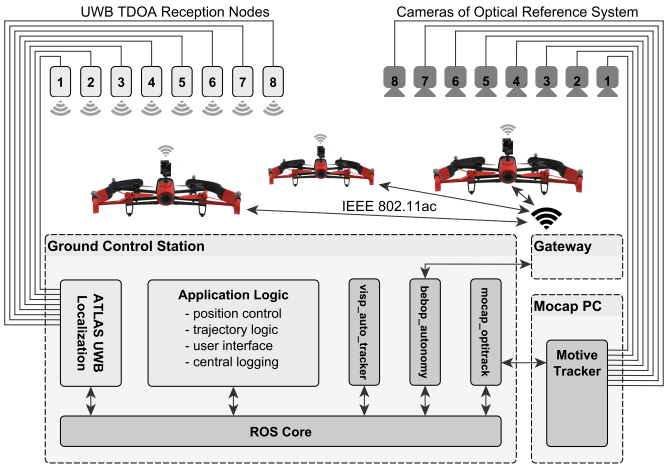

Fig. 3. Topology block diagram of the overall experimental setup depicting the interaction of the individual software and hardware components.

TABLE I. Positions of the anchors used in the experiments.

anchor	sync	1	2	3	4	5	6	7	8
x $[m]$	-1.11	-1.11	-1.17	1.20	3.54	3.54	3.42	1.20	-1.17
y $[m]$	0.00	0.00	-3.49	-3.49	-3.45	0.02	3.52	3.49	3.49
z $[m]$	1.85	2.05	0.29	2.43	2.55	2.08	0.28	2.16	2.17

The previously developed ATLAS UWB localization system [14] is used as the basis for absolute positioning in the depicted setup. A set of eight receiving nodes is distributed spatially in the laboratory. The exact positions of those anchor nodes are listed in Tab. I. When acting as a localization tag the node is simply transmitting packets in a random interval with a predefined mean to avoid collisions. Similar to the localization tag, the synchronization node is only transmitting packets. However, it is doing so with a predefined precise interval to enable clock reconstruction. For the experiments, a synchronization frequency of 10 Hz was chosen. Anchors however, simply receive packets, mark their precise TOA based on their local clock and communicate those received packets over the backbone protocol. The basis for positioning is the TOA timestamp which is a 40-bit integer, where one bit corresponds to $1s/(128 \cdot 499.2 \cdot 10^6)$. All received packets are transmitted over the backbone. In our laboratory setup plain serial over USB is used. Note that the backbone is not distributing a common clock.

TABLE II. Channel configuration used in the experiments.

f_c [GHz]	B [MHz]	n_{prc}	f_{pr} [MHz]	R [kbps]	c_{pr}	n_{pr}
6.4896	499.2	127	62.4	850	9	256

Due to the individual clock drift of each anchor, accurate clock synchronization is needed for precise localization [12]. Therefore, wireless clock synchronization through a dedicated node is used. The known periodicity of those synchronization packets enables the central localization server to reconstruct the individual relative clock offsets and drifts of each anchor node clock. The clock models for each anchor n are used, to extrapolate the clock offset $\varepsilon_{n,i}$ at the reception of a positioning frame i. The clock offset $\varepsilon_{n,k} = t_{sn,k} - t_{r,k}$ at each synchronization step k is the difference of the time of the reference clock $t_{r,k}$ and the measured TOA of the synchronization frame $t_{sn,k}$. The clock drift $\dot{\varepsilon}_{n,k}$ is used to extrapolate and finally correct the measured TOAs $t_{n,i}$ of the positioning frame, see (1).

$$\varepsilon_{n,i} = \varepsilon_{n,k} + \dot{\varepsilon}_{n,k}(t_{n,i} - t_{sn,k}) \tag{1}$$

To minimize the effect on the positioning results, the drift needs to be extrapolated between the reception of two frames. After clock correction, the samples are processed through an outliers detection that discards samples where the change or absolute value of the TDOAs is greater or smaller than a static threshold. In the case of this work the absolute threshold was $100\,\mathrm{ns}$ and the threshold for TDOA change was chosen as $6.7\,\mathrm{ns/s}$. This enables the system to estimate the position of the mobile node through the TDOA at the anchors. For position estimation an extended Kalman filter (EKF) is used as extensively described in [14]. The ATLAS application was modified to interface with ROS enabling seamless integration with the other components of the setup.

The position controller is structured as depicted in Fig. 4. The desired position $\mathbf{P}_d = [x_d,\ y_d]^T$ is the control input for the outer loop. The actual position $\mathbf{P} = [x,\ y]^T$ is measured through the position measurement system function $\mathbf{H}_p$ to obtain the estimated position $\hat{\mathbf{P}}$ which is subtracted from $\mathbf{P}_d$ to obtain the current position error. The error is used by the control algorithm to obtain the desired velocity command $\dot{\mathbf{P}}_d$ to the inner loop. A limiter is used to ensure that those commands stay within a safe range defined by $\dot{p}_{max}$. The optical flow sensor determines the drone's measured velocity

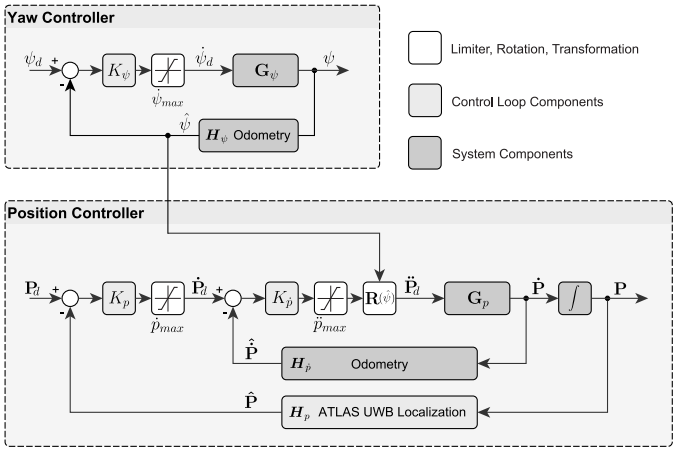

Fig. 4. Block diagram of the cascaded loop for UAV position control. Note that the position and velocity feedback $\mathbf{H}_p$ and $\mathbf{H}_{\dot{p}}$ can be provided by either odometry, the UWB system or the optical reference system.

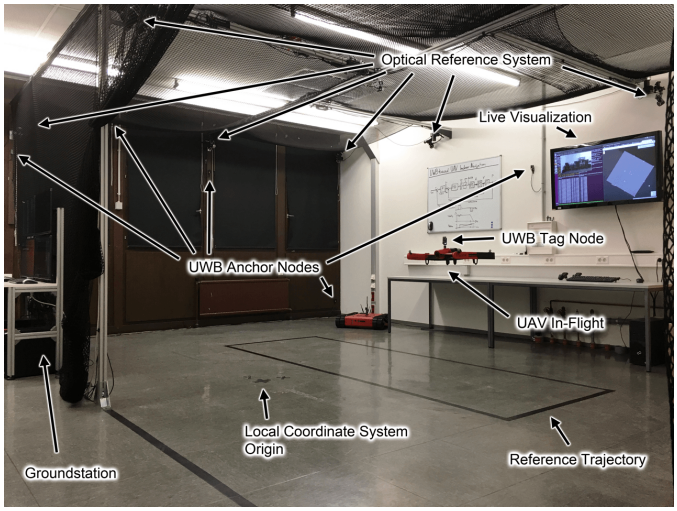

Fig. 5. Photo of the experimental setup showing the optical reference system, the UWB anchor nodes, the in-flight UAV equipped with the UWB tag node, the groundstation, the live visualization and the reference trajectory.

$\hat{\mathbf{P}}$ by measuring the true velocity $\dot{\mathbf{P}}$ through $\mathbf{H}_{\dot{p}}$. The measured velocity is subtracted from the desired velocity $\dot{\mathbf{P}}_d$, this velocity error is guaranteed not to exceed the predetermined value $\ddot{p}_{max}$ analogueously by using a controller limiter. The obtained acceleration commands $\ddot{\mathbf{P}}_d$ are in the controller coordinate frame and are then transfered to the local coordinate frame of the drone in order to get the actual commands for roll φ and pitch θ. That is done by multiplying with the rotation matrix $\mathbf{R}(\dot{\psi})$ around the estimated yaw angle $\dot{\psi}$.

III. Experimental Evaluation

In order to evaluate the system's performance, a series of experiments were performed. The state of the drone in form of its odometry, the calculated UWB position estimation, the control loop setpoints and the reference pose obtained through the motion capture system are recorded centrally by the application performing the control loop. The logfiles of those experiments are provided alongside this work [18]. A video of a practical demonstration of UWB-based UAV indoor navigation in the context of this paper is available online [19].

A. Control Loop Tuning

In a first experiment the setpoint for position control of the drone is alternated two times between the following waypoints: $\mathbf{W}_{P1} = [1.2, 1.8]^T$ and $\mathbf{W}_{P2} = [1.2, -1.8]^T$ along the y-axis. In this setup, the ATLAS UWB system is used for position feedback $\mathbf{H}_p$. The odometry based on the inertial measurement unit (IMU) and the optical flow sensor is used for velocity feedback $\mathbf{H}_{\dot{\mathbf{P}}}$ and yaw feedback $\mathbf{H}_\psi$. The parameters for the control loop were determined using Ziegler-Nichols and are listed in Tab. III.

TABLE III. Control Loop Parameters.

$K_{p,p}$	$K_{p,i}$	$K_{p,d}$	$\dot{p}_{max}$	$K_{\dot{p},p}$	$K_{\dot{p},i}$	$K_{\dot{p},d}$	$\ddot{p}_{max}$	K_ψ	$\dot{\psi}_{max}$
0.6	0.0	0.0	0.4	0.4	0.001	0.001	0.4	1.0	0.5

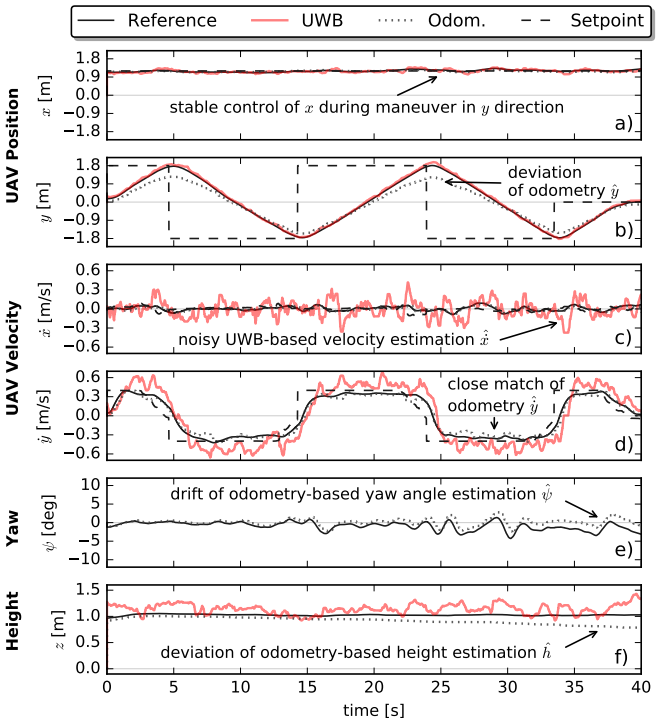

Fig. 6. Time-series of the experimental recordings used to tune the position controller. Note that different possible inputs for the control loop are depicted, showing the trade-offs for each system.

The resulting movement is depicted in Fig. 6. In order to show the functionality of the control loop, the position of the UAV, the velocity and the orientation are visualized. It can be seen that the UAV is capable of following the setpoints defined through $\mathbf{W}_{P1}$ and $\mathbf{W}_{P2}$. The stability along the x-axis is depicted a). In b), the alternation between the two setpoints along the y-axis is visible. The localization accuracy of the UWB-based system compared to the optical reference system is clearly visible in the graphs. Note the deviation of the position estimation through the odometry compared to the reference system and the UWB-based position estimation.

Figures c) and d) depict the estimated and true components of the velocity $\dot{\mathbf{P}}$ of the UAV $\dot{x}$ and $\dot{y}$. It is clearly visible, that the UWB-based velocity estimation follows the true velocity measured by the reference system. However, it inherits a significant amount of noise, decreasing the performance of the inner velocity-based control loop. Therefore, the odometry-based velocity was chosen as the feedback system $\mathbf{H}_{\dot{p}}$ for the inner loop.

In e) and f) the yaw angle ψ and the height z are shown respectively. The yaw angle is only available from the odometry, as the UWB system can only provide a three-dimensional pose and no orientation. However, odometry based yaw and height estimations are prone to long-term drift which is clearly visible. Whereas, the height estimation of the UWB system, though noisy does not suffer from from long-term drift. The anchor constellation, which is optimized for horizontal and not vertical positioning causes the noisy height estimation.

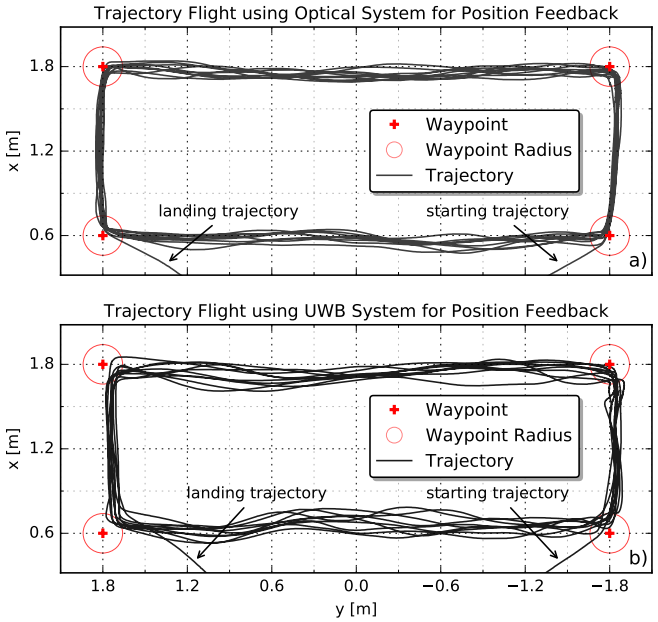

Fig. 7. Resulting trajectories in a top-down view. The upper figure shows the position control using the optical reference system, the lower figure uses the UWB system for position feedback and the odometry for velocity estimation.

B. Repeatability & Long-Term Stability

To show the long-term stability and repeatability of the proposed system, a second experiment is conducted. The drone is programmed to perform a trajectory ten times in a row through the following waypoints: $\mathbf{W}_{P3} = [0.6, -1.8]^T$, $\mathbf{W}_{P4} = [1.8, -1.8]^T$, $\mathbf{W}_{P5} = [1.8, 1.8]^T$ and $\mathbf{W}_{P6} = [0.6, 1.8]^T$. In this experiment, the UWB system is used for position feedback $\mathbf{H}_p$, the odometry is used for velocity estimation $\mathbf{H}_{\dot{p}}$ and the optical reference system is used for yaw feedback $\mathbf{H}_\psi$, due to the lack of reliable long-term stability of the odometry-based yaw estimation. The control loop parameters are listed in Tab. III.

In order to set a baseline for position control, another experiment similar to the abovementioned one is conducted. The optical reference system is used here for both position feedback $\mathbf{H}_p$ and velocity estimation $\mathbf{H}_{\dot{p}}$. The experiment still utilizes the same control parameters as the first one. The results of the flight trajectory using the optical system for

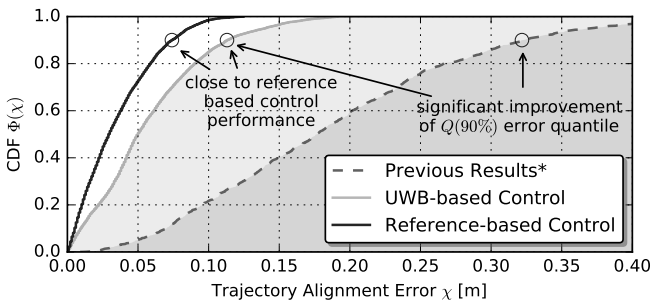

Fig. 8. Cumulative distribution functions $\Phi(\chi)$ of the absolute lateral deviation χ of the true trajectory from the reference trajectory for the reference-based and UWB-based position control respectively. * [13]

position feedback compared to those using the UWB-based position feedback are depicted in Fig. 7. Both approaches achieve quite good trajectory repeatability. As expected, the trajectories using the optical reference system perform slightly better. However, even though the reference system provides the control loop with positions accurate in the sub-millimeter range, perfect trajectory following is not possible. This is due to environmental disturbances and the limited control interface provided by the drone SDK.

To quantify the accuracy of the trajectory following, the cumulative distribution function (CDF) $\Phi(\chi)$ of the lateral error χ to the reference trajectory through all waypoints is depicted in Fig. 8. It is clearly observable that the preformance of the UWB-based position control is close to that of the reference-based control. Therefore, it can be concluded that the proposed approach for scalable high-precision UAV position control using TDOA-based UWB localization is feasible. In order to set a baseline, the experimental results of previous work [13] are used. It should be noted that the error from previous results is the deviation from a position-hold experiment using an emulated GNSS receiver and a black box position control loop from a commercial UAV. The GNSS emulation was done using a SDS-TWR based UWB system and onboard processing. Nevertheless, as position hold is expected to perform better than dynamic flight, those results are used to illustrate the progress compared to previous work.

C. Proposed Scalable Multi-UAV Control

In order to show the proposed system's core capability of scalable multi-user integration, a third experiment is conducted. Three UAVs simultaneously follow an eight-shaped trajectory through the waypoints listed in Tab. IV in the laboratory setup. The UAVs take off at the 1st, the 7th and the 13th waypoint for UAV 1, 2 and 3 respectively, follow the trajectory three times and land automatically. Each UAV is equipped with a UWB tag transmitting within a uniformly distributed random time interval betweeen $10\,\mathrm{ms}$ and $35\,\mathrm{ms}$ resulting in a mean update rate of more than $40\,\mathrm{Hz}$. The random channel access was chosen to provide all accessing participants with the same prerequirements and enable fair competition in terms of channel utilization. Like in section III-B, the UWB position is used as the basis for position control and the odometry for velocity estimation.

The top trajectories of the individual UAVs in simultaneous flight are depicted in Fig. 9. The eight-shaped reference trajectory is clearly visible in all three plots. Also depicted are the desired waypoints, the waypoint catching radius and the estimated trajectory obtained through the UWB system. It should be noted that UAV 1 and 2 are the first generation Bebop drones, whereas UAV 3 is a second generation Bebop.

TABLE IV. WAYPOINTS OF THE MULTI-UAV TRAJECTORY

waypoint	1	2	3	4	5	6	7	8	9	10
x $[m]$	1.20	0.75	0.60	0.60	0.75	1.20	1.65	1.80	1.80	1.65
y $[m]$	0.00	0.30	0.75	1.20	1.65	1.80	1.65	1.20	0.75	0.30
waypoint	11	12	13	14	15	16	17	18	19	20
x $[m]$	0.75	0.60	0.60	0.75	1.20	1.65	1.80	1.80	1.65	1.20
y $[m]$	-0.30	-0.75	-1.20	-1.65	-1.80	-1.65	-1.20	-0.75	-0.30	0.00

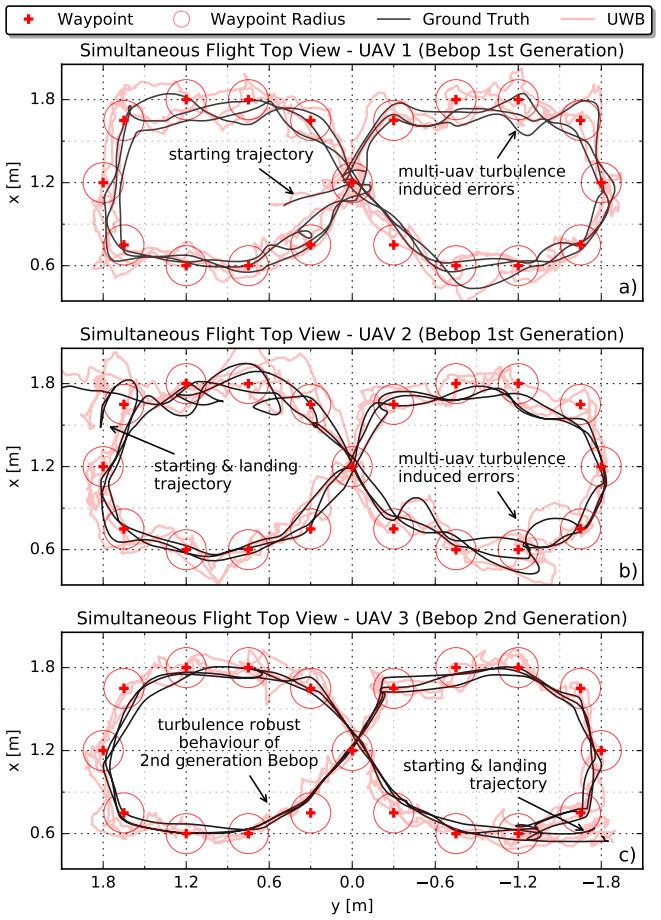

Fig. 9. Simultaneous trajectories in a top-down view. Note the difference between the 1st generation Bebop and the 2nd generation which is less susceptible to the turbulences introduced by the other flying UAVs.

This is clearly visible in the ground truth of the experimental results as the second generation is less prone to multi-UAV turbulences in close proximity. Aside from the turbulence-induced disturbances however, all three UAVs are capable of repeatably following the predefined trajectory in a synchronized and stable manner.

To quantify the multi-user capability, the CDF $\Phi(\tau)$ of the achieved inter-arrival times τ (IAT) of the UWB-based

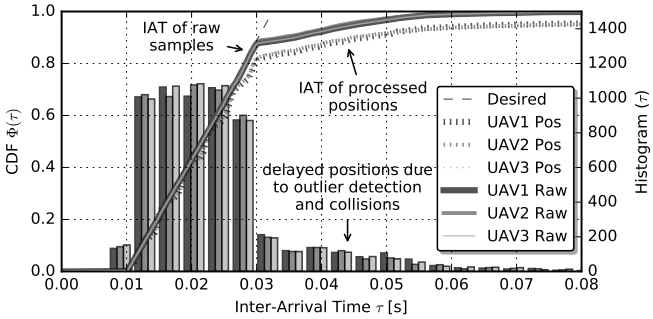

Fig. 10. Cumulative distribution functions $\Phi(\tau)$ of the inter-arrival times τ for each UAV. Note the uniform distribution in the histogram of the inter-arrival times and the difference between raw samples and processed positions.

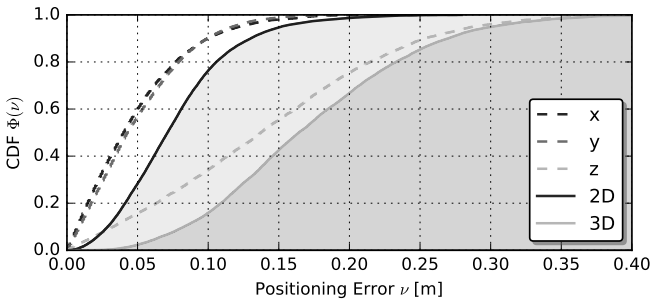

Fig. 11. Cumulative distribution functions $\Phi(\nu)$ of the absolute euclidean error ν of the UWB positioning results. Note the difference between horizontal and vertical positioning accuracy induced by the anchor topology.

positioning results are depicted Fig. 10. The linear shape of the uniform random distribution used for channel access is clearly recognizable in the CDFs of all UAVs. Furthermore it can be seen, that all CDFs are very close to each other, proving the resulting equality of proposed channel access scheme. However, not all packets transmitted by the UWB tag are used to calculate the transmitters position in the TDOA-based system. Outlier detection is used to improve the overall positioning performance in a two-stage process as described in section II. Furthermore, a positioning sample is rejected if not received by all anchors in the given setup. Therefore, a relatively large amount of positions have a greater IAT than desired.

TABLE V. IAT QUANTILES FOR THE INDIVIDUAL UAVS.

UAV	$Q(50\%)$ [s]	$Q(75\%)$ [s]	$Q(90\%)$ [s]	$Q(95\%)$ [s]	$Q(99\%)$ [s]	samples
1 Pos	0.022	0.029	0.047	0.072	0.334	6401
2 Pos	0.022	0.029	0.044	0.077	0.340	6389
3 Pos	0.022	0.029	0.045	0.073	0.332	6441
1 Raw	0.022	0.027	0.036	0.046	0.061	9203
2 Raw	0.022	0.027	0.034	0.043	0.059	9307
3 Raw	0.021	0.027	0.035	0.045	0.061	9300

In order to visualize this effect, the IATs of the raw and unprocessed samples are compared to the IATs of the processed positions in Fig. 10. The corresponding IAT quantiles are listen in Tab. V to make the results comparable. The effect of outlier detection is most notably visible comparing the $99\,\%$ quantiles. The raw samples achieve a maximum IAT in $99\,\%$ of all cases of under $62\,\mathrm{ms}$. The processed positions however, can only guarantee an IAT of under $341\,\mathrm{ms}$. This is simply due to the rejection of a subset of samples. We expect to decrease the amount of rejections through more intelligent filtering in the future. Part of that filtering will be a more robust wireless clock synchronization using more elaborate clock models. Another aspect will be dynamic and adaptive sample quality assessment

TABLE VI. LOCALIZATION ERROR QUANTILES FOR THE INDIVIDUAL AXES, THE HORIZONTAL PLANE AND THE POSITIONAL SPACE.

	$Q(50\%)$ [m]	$Q(75\%)$ [m]	$Q(90\%)$ [m]	$Q(95\%)$ [m]	$Q(99\%)$ [m]	samples
x	0.040	0.069	0.100	0.123	0.168	28938
y	0.043	0.072	0.100	0.118	0.152	28938
z	0.137	0.199	0.254	0.288	0.357	28938
2D	0.071	0.098	0.130	0.152	0.209	28938
3D	0.164	0.219	0.270	0.301	0.365	28938

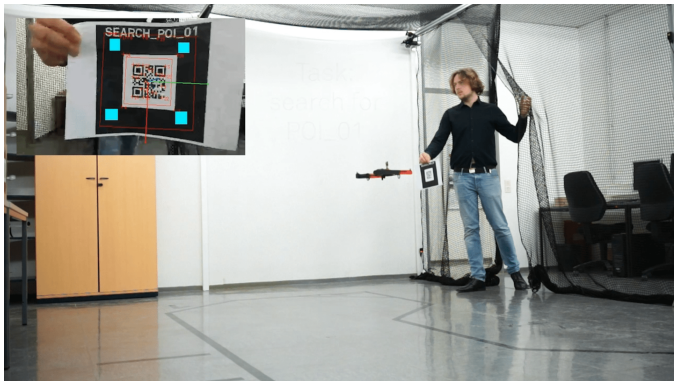

Fig. 12. Application demonstration video [19]. The user is commanding the UAV to search for a specific QR-code labeled box in an unsorted warehouse.

and weighing based on additional information obtained from the receiver.

However, we could show that even with a conservative channel configuration used during the experiments listed in Tab. II we can provide a mean update rate of more than $40\,\mathrm{Hz}$ for three UAVs simultaneously. Using a scheduled TDOA-based channel access scheme and more aggressive channel configurations, the number of simultaneously flying UAVs can be increased even to more than 100 in the future.

In order to further characterize the quality of the positioning results contributed by the UWB positioning system in the third experiment, the absolute euclidean positioning errors of all three UAVs are analyzed. The CDFs of the errors are depicted in Fig. 11. The individual absolute errors along each axis are depicted next to the absolute euclidean horizontal ν_H and positional ν_P error. It is clearly visible, that the constellation of anchors is optimized for horizontal positioning. Horizontal accuracy is preferred as the height control of UAVs is usually based on ultrasonic sensing in close proximity to the ground and barometric sensing in the far field. The achieved error quantiles are also listed in Tab. VI for comparison.

D. Interactive Application

To prove the general applicability of the proposed approach, an example application compromising a single UAV is presented. In the given scenario, which is also represented in

Fig. 13. Still of the interactive application video [19]. The UAV is searching for a QR-code labeled box in the warehouse-mockup.

the demonstration video [19] provided alongside this work, the UAV has to determine the location of a user-defined box in an unsorted warehouse (in this case a small setup in our laboratory). Therefore, the user provides the UAV with a searching point of interest (POI) through a QR-code as depicted in Fig. 12. The UAV is then following a predefined trajectory covering the location of all boxes in the warehouse, see Fig. 13. Once found, the drone notifies the user by oscillation around the roll-axis and awaits further commands. Although just a scaled scenario is evaluated, the experiment proves that the proposed approach enables flexible use of UAVs indoors for information collection. The proposed system is refitted easily in existing environments and may help to enable cost and time-effective stocktaking or similar applications such as depicted by Fig. 1.

IV. Conclusion and Future Work

This paper presents an approach for UAV indoor navigation using a TDOA-based UWB indoor localization system. The system is build upon open-source components and uses a low-cost commercial off-the shelf drone with minor modifications to carry a UWB node. All aspects of the proposed system were covered in detail and its performance was experimentally analyzed. It was shown that the system is capable of robust trajectory following with a close to ground-truth based performance in terms of trajectory deviation. The multi-user capabilities were proven by showing a simultaneous flight of three UAVs in a challenging space-constraint environment and a detailed inter-arrival time analysis. The raw samples, localization results [18] and a video [19] demonstrating the performance of the system are provided alongside this work.

Future work may include calibration of the odometry using the front-facing camera and improving localization accuracy through advanced sensor fusion considering inertial sensors and UWB-specific channel response analysis.

Acknowledgement

The work on this paper has been partially funded by Deutsche Forschungsgemeinschaft (DFG) within the Collaborative Research Center SFB 876 “Providing Information by Resource-Constrained Analysis”, project A4 and was supported by the federal state of Northrhine-Westphalia and the “European Regional Development Fund” (EFRE) 2014-2020 in the course of the CPS.HUB/NRW project under grant number EFRE-0400008. We also thank Ole Feldmeier for his support with the initial setup.

References

[1] G. Ducard and R. D’Andrea. Autonomous quadrotor flight using a vision system and accommodating frames misalignment. In *Industrial embedded systems, 2009. SIES’09. IEEE international symposium on*, pages 261–264. IEEE, 2009.

[2] N. Michael, D. Mellinger, Q. Lindsey, and V. Kumar. The GRASP multiple micro-UAV testbed. *IEEE Robotics Automation Magazine*, 17(3):56–65, Sep 2010.

[3] A. Kushleyev, D. Mellinger, C. Powers, and V. Kumar. Towards a swarm of agile micro quadrotors. *Autonomous Robots*, 35(4):287–300, 2013.

[4] S. Lupashin, M. Hehn, M. W. Mueller, A. P. Schoellig, M. Sherback, and R. D’Andrea. A platform for aerial robotics research and demonstration: The flying machine arena. *Mechatronics*, 2014.

[5] B. Kempke, P. Pannuto, and P. Dutta. Polypoint: Guiding indoor quadrotors with ultra-wideband localization. In *Proceedings of the 2nd International Workshop on Hot Topics in Wireless*, HotWireless ’15, pages 16–20, New York, NY, USA, 2015. ACM.

[6] B. Kempke, P. Pannuto, and P. Dutta. Harmonium: Asymmetric, bandstitched UWB for fast, accurate, and robust indoor localization. In *2016 15th ACM/IEEE International Conference on Information Processing in Sensor Networks (IPSN)*, pages 1–12, Apr 2016.

[7] C. Hui, C. Yousheng, and W. W. Shing. Trajectory tracking and formation flight of autonomous UAVs in GPS-denied environments using onboard sensing. In *Proceedings of 2014 IEEE Chinese Guidance, Navigation and Control Conference*, pages 2639–2645, Aug 2014.

[8] K. Hausman, S. Weiss, R. Brockers, L. Matthies, and G. S. Sukhatme. Self-calibrating multi-sensor fusion with probabilistic measurement validation for seamless sensor switching on a UAV. In *Robotics and Automation (ICRA), 2016 IEEE International Conference on*, pages 4289–4296. IEEE, 2016.

[9] Kexin Guo, Zhirong Qiu, Cunxiao Miao, Abdul Hanif Zaini, Chun-Lin Chen, Wei Meng, and Lihua Xie. Ultra-wideband-based localization for quadcopter navigation. *Unmanned Systems*, 04(01):23–34, 2016.

[10] M. W. Mueller, M. Hamer, and R. D’Andrea. Fusing ultra-wideband range measurements with accelerometers and rate gyroscopes for quadrocopter state estimation. In *2015 IEEE International Conference on Robotics and Automation (ICRA)*, pages 1730–1736, May 2015.

[11] A. Ledergerber, M. Hamer, and R. D’Andrea. A robot self-localization system using one-way ultra-wideband communication. In *Intelligent Robots and Systems (IROS), 2015 IEEE/RSJ International Conference on*, pages 3131–3137, Sep 2015.

[12] J. Tiemann, F. Eckermann, and C. Wietfeld. Multi-user interference and wireless clock synchronization in TDOA-based UWB localization. In *2016 International Conference on Indoor Positioning and Indoor Navigation (IPIN)*, Alcala de Henares, Madrid, Spain, Oct 2016.

[13] J. Tiemann, F. Schweikowski, and C. Wietfeld. Design of an UWB indoor-positioning system for UAV navigation in GNSS-denied environments. In *Indoor Positioning and Indoor Navigation (IPIN), 2015 International Conference on*, Oct 2015.

[14] J. Tiemann, F. Eckermann, and C. Wietfeld. ATLAS - an open-source TDOA-based ultra-wideband localization system. In *2016 International Conference on Indoor Positioning and Indoor Navigation (IPIN)*, Alcala de Henares, Madrid, Spain, Oct 2016.

[15] M. Quigley, K. Conley, B. P. Gerkey, J. Faust, T. Foote, J. Leibs, R. Wheeler, and A. Y. Ng. ROS: an open-source robot operating system. In *ICRA Workshop on Open Source Software*, 2009.

[16] M. Monajjemi, S. Mohaimenianpour, and R. Vaughan. UAV, come to me: End-to-end, multi-scale situated hri with an uninstrumented human and a distant UAV. In *Intelligent Robots and Systems (IROS), 2016 IEEE/RSJ International Conference on*, pages 4410–4417. IEEE, 2016.

[17] E. Marchand, H. Uchiyama, and F. Spindler. Pose estimation for augmented reality: a hands-on survey. *IEEE Trans. on Visualization and Computer Graphics*, 22(12):2633–2651, Dec 2016.

[18] J. Tiemann. Raw experimental localization, sample and tracking data, http://dx.doi.org/10.5281/zenodo.571794. May 2017.

[19] J. Tiemann. Scalable and precise multi-UAV indoor navigation using TDOA-based UWB localization, video: https://vimeo.com/205754093. 2017.